Externally controlled attractor selection in a high-dimensional system

Frederick H. Willeboordse*
Department of Physics, The National University of Singapore, Singapore 119260

Kunihiko Kaneko†
Department of Pure and Applied Sciences, University of Tokyo, Komaba, Meguro-ku, Tokyo 153-8902, Japan, and ERATO Complex Systems Biology Project, JST 3-8-1 Komaba, Meguro-ku, Tokyo 153-8902, Japan
(Received 2 February 2005; published 15 August 2005)

A high-dimensional dynamical system with global couplings that can serve as a prototype for systems with very large numbers of attractors like memory is investigated and shown to be controllable by external inputs. By changing the duration that noise is added, final attractors are selected as the number of degrees of freedom of the nonsynchronized elements decreases one by one over time. Furthermore, it is found that this selection of attractors is also possible by controlling the sweeping speed of a parameter. The mechanism for this controlled selection is explained and shown to be rather general. Applications to attractor switching are given.

DOI: 10.1103/PhysRevE.72.026207 PACS number(s): 05.45.Jn, 05.45.Ra

I. INTRODUCTION

High-dimensional dynamical systems with many degrees of freedom are often characterized by large numbers of attractors. The ability to control and select these attractors is of great importance, not only from a fundamental point of view, but also for wide-ranging practical applications.

Consider, for example, memory. In neural network studies, it is often represented as an attractor in a dynamical system with a large number of attractors. The recall of a memory can then be thought of as due to an externally triggered attractor switch [1]. In other words, the input acts as an external control that leads to the selection of an attractor that is output as a memory. In the case of neural networks (be they artificial or natural), memory is directly related to information processing. However, controlled attractor selection is not only relevant in this particular context. An example of another kind of memory is given by cell states that can be represented as attracting chemical reaction dynamics [2,3]. Quite generally, as long as a memory can be considered an attractor, the selection of this attractor by external inputs and hence external control is important.

An interesting concept regarding phase space structures and the selection of stable states was recently proposed in relation to protein folding. It is the notion of phase space funnels. The question of how proteins form a folded state (with a specific function) is studied in the field of protein folding and the concept of funnels was introduced to understand a selection process where the minimum state is reached through a series of metastable states whose energy landscape is organized in a funnel-like manner [4]. The key point being that the ordering of the metastable states according to their energy levels is strongly related to the ordering of attractors in phase space. If such an ordered structure exists in a high-dimensional system, even if it does not directly contain a quantity that can be considered an "energy," it should be suitable for attractor control since the addition of a simple input signal or of some noise could lead to the successive selection of attractors according to the ordering. How far it will proceed in this successive selection will then depend on the duration and amplitude of the input or noise.

It is therefore of significant interest to study the switching of attractors in high-dimensional systems by external operations, and this has been discussed, e.g., in the context of Boolean networks [2,5], neural networks [2], cellular automata [6] and open-flow coupled map lattices [7,8]. Here we consider a dissipative high-dimensional system with many attractors and investigate how attractors can be selected just by adding noise.

Levels of organization among huge numbers of attractors have been studied in depth in globally coupled maps (GCM) [9–13] that share many properties with spin glasses like those in the Sherrington-Kirkpatrick model [14], which is a thoroughly investigated thermodynamical system displaying many different metastable states. On the other hand, the relevance of multiple attractors and of the chaotic itinerancy observed in GCM to neural dynamics has been discussed over a decade [15].

Externally triggered attractor switching as well as basin structures were previously also studied in a standard type of GCM, but the behavior turned out to be too complicated for controlled attractor selection [16–18], while a study investigating the influence of noise on the preference of attractors in a highly multistable system was carried out for a low-dimensional model [19].

Nevertheless, owing to their proven usefulness as tools for analyzing complex phenomena, it is of great interest to find a prototype GCM in which attractor switching can be controlled. In this paper it will be shown that this can be achieved by a well-motivated modification of a generally studied globally coupled map. Thus, we believe that the model described here can serve as a prototype for attractor switching in high-dimensional systems.

*Electronic address: willeboordse@yahoo.com; URL: http://www.willeboordse.ch/science/
†Electronic address: kaneko@complex.c.u-tokyo.ac.jp; URL: http://chaos.c.u-tokyo.ac.jp/

This paper is organized as follows: in Sec. II we describe the model studied and introduce its four basic phases. The suprising influence of noise on where these phases occur is presented in Sec. III, and an application of this finding as with regards to attractor control in Sec. IV. The mechanism is investigated and explained in Sec. V while the conclusion is given in Sec. VI.

II. MODEL

In general, a globally coupled map can be expressed as

$$x_{n+1}^i = (1-\varepsilon) f(x_n^i) + \frac{\varepsilon}{N} \sum_{j=1}^{N} g(x_n^j), \tag{1}$$

with $f(x_n^i)$ the local map and $g(x_n^i)$ a map applied to the elements coupled to. The subscript n and superscript i indicate the discrete time and element, respectively, while N is the system size and ε the coupling constant. The case where $g(x)=f(x)$ has widely been studied [9–13], but, as such, f and g need not be identical.

Indeed, when $g \neq f$, the fundamental relationship between coupling and instability can be reversed from the case when $g=f$. When $g=f$, the coupling term has a stabilizing effect and consequently a single element in isolation is more chaotic than the coupled system [9], whereas when $g \neq f$, as will be shown here, a single element or the synchronized state can be periodic while the coupled system is chaotic.

As an example of such system where $g \neq f$, we take the simple case $g(x)=x$, a model that has occasionally been studied in the context of synchronization (see, e.g., [20]). For f we choose the logistic map $f(x_n)=x_{n+1}=1-\alpha x_n^2$, with α the nonlinearity.

As usually done for globally coupled maps, elements are grouped into clusters that oscillate in unison, taking (nearly) identical x values. The clusters N_j are numbered from large to small such that N_1 is the largest cluster, and one has $(N_1, N_2, \ldots, N_k)$ with $\Sigma_{j=1}^{k} N_j = N$. With regards to the clusters, the main phases that exist for the various parameter regimes are as follows: a synchronized phase where all the elements oscillate in unison, an ordered phase characterized by a small number of large clusters, a partially ordered phase in which some large clusters coexist with many small clusters, and a turbulent phase where the average cluster size is one. In other words, the phases are defined in the following way: $k=1$ (coherent phase), $1<k=o(N)$ (ordered phase), $k=O(N)<N$ (partially ordered phase), and $k=N$ (turbulent phase). Typical examples of these phases are shown in Fig. 1, where the x axis denotes an element's index and the y axis its value. As the coupling in Fig. 1 is global, the spatial ordering of the sites is, of course, arbitrary. Nevertheless, it is useful to be able to see all the x values at once, as it can reveal a possible underlying structure (like, e.g., remnants of the local map's band structure).

III. PHASES AND NOISE

In order to find out where the basic regimes are located in parameter space, phase diagrams with and without the temporary addition of noise are shown in Figs. 2(a) and 2(b). After preparing the system with random initial conditions $x \in [-1,1]$, a transient of 10^4 time steps was discarded before either temporarily adding noise and then determining the number of clusters k, or determining the number of clusters right away.

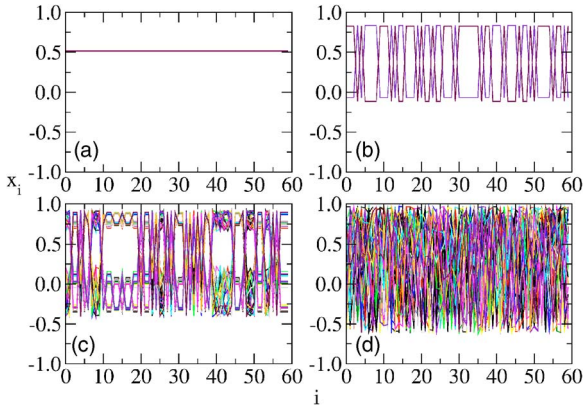

FIG. 1. (Color online). The four main phases of the model for $\alpha=1.8$ and $N=60$. Fifty consecutive time steps are overlaid after a transient of 10^5 time steps. (a) Synchronized phase: $\varepsilon=0.5$, $N_1=60$; (b) ordered phase: $\varepsilon=0.25$, $N_1=34, N_2=26$; (c) partially ordered phase: $\varepsilon=0.14$, $N_1=21$, $N_2=13$, $N_{4-28}=1$; (d) turbulent phase: $\varepsilon=0.06$, $N_{1-60}=1$. It should be noted that the x axis does not represent space and merely represents the element index.

Unless mentioned otherwise, the temporary addition of noise is carried out in the following way: After the transient, first noise is added for 10^3 time steps and then the system is evolved for another 10^3 time steps in order to allow it to reach a possible attractor. For each time step that the noise is applied, equiprobable random numbers between plus and minus the noise percentage are added to all the elements x_i, subjected to the condition that $-1 \leqslant x_i \leqslant 1$.

As such, the phase diagram of Fig. 2(a) does not differ much from that of the standard GCM where $g(x_n^i)=f(x_n^i)$, but in the standard GCM case the phase diagram (corresponding to Fig. 2(b)) changes only very little when noise is added temporarily. By contrast, the difference between Figs. 2(a) and 2(b) is striking. In particular, the coherent phase region expands drastically (roughly by a factor 10) when noise is added. Indeed, the remarkable fact is that noise enhances rather than impedes synchronization.

Next it is investigated how this selection of attractors depends on the duration that noise is applied. Figures 3(a) and 3(b) show the number of clusters in the final state versus the number of time steps that noise is temporarily added to the system.

It can be seen that, on average, almost any time duration significantly decreases the number of clusters. In particular, after some time, the number of clusters of the selected attractor decreases one by one with time over a rather long interval.

Basically, the scenario of reaching the synchronized state is as follows: When noise has been added only for a short time, some big clusters are formed that coexist with a very large number of small clusters or desynchronized elements. Then, while the time the noise is added increases, the num-

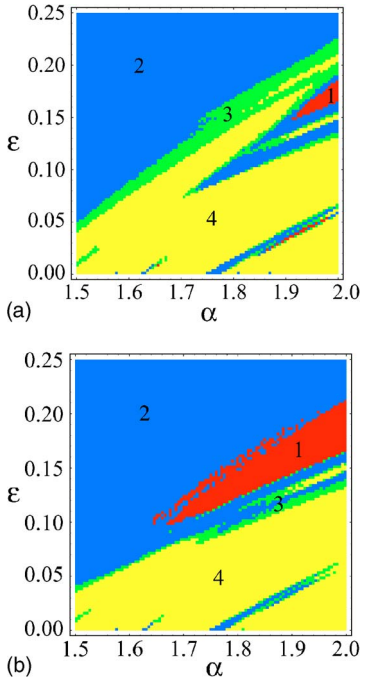

FIG. 2. (Color online). (a) Phase diagram without the temporary addition of noise. (b) Phase diagram with the temporary addition of 5% noise. The major regions are indicated by (1) synchronized phase (red), (2) ordered phase (blue), (3) partially ordered phase (green), and (4) turbulent phase (yellow). The phase is derived by counting the total number of clusters k and making the following correspondences: $k=1\rightarrow$synchronized phase, $1<N_k \leqslant 10\rightarrow$ordered phase, $10<k\leqslant 30\rightarrow$partially ordered phase, $k>30\rightarrow$turbulent phase. (More strictly speaking, $k\approx N$ in the turbulent phase. However, as the case for $k>30$ should not be counted as a partially ordered phase but should not be ignored either, it was grouped with the turbulent phase). The system size was set to $N=60$. Elements are considered to be in the same cluster when their values differ by no more than 10^{-5}.

ber of large clusters gradually decreases, even though the total number of clusters may spike in between when the state changes, e.g., from a state with five large clusters to a state with four large clusters. Besides contributing to the remaining clusters, the disappearing cluster may split into many small clusters, until each of its elements is desynchronized ($N_j=1$). Eventually, for $\alpha=1.77$, there is a single large cluster coexisting with many desynchronized elements [i.e., $(N_1,1,1,1,\ldots 1)$], while for $\alpha=1.70$, two large clusters coexist to form $(N_1,N_2,1,1,1,\ldots,1)$. After these states are reached, desynchronized elements are absorbed into a large cluster one by one with the help of noise. In the former case, this successively leads to switches $(N_1,1,\ldots,1,1,1)\rightarrow(N_1+1,\ldots,1,1)\rightarrow(N_1+2,\ldots,1)$, while in the latter case, switches occur yielding either $(N_1+1,N_2,1,1,\ldots,1)$ or $(N_1,N_2+1,1,1,\ldots,1)$, and when all the small clusters are gone, N_1 and N_2 merge so that eventually a single coherent cluster is left.

Inevitably, the amount of noise added will have some influence. Figure 4 shows the average number of clusters versus the nonlinearity for various noise levels given a coupling strength where the noise levels distinctively influence the

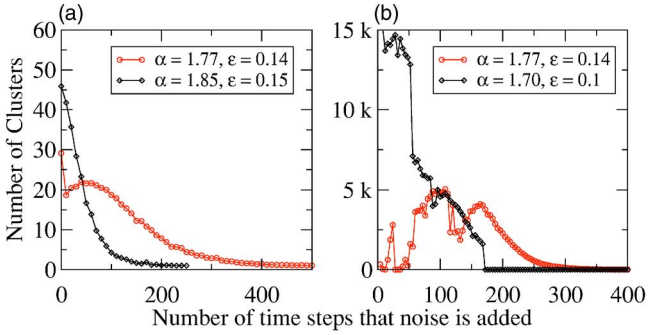

FIG. 3. (Color online). The number of clusters versus the time the noise is added. The phase was determined, and the noise added in the same fashion as for the phase diagram, Fig. 2(b) (except that the duration the noise is added is given by the x axis). The number of clusters was determined every 4th time step by making a copy of the state of the system and evolving it for 1000 time steps before determining the number of clusters. $N=60$. (a) The average of 10^3 runs was taken for each data point and the noise level was 5%. (b) Two individual runs. For $\alpha=1.7$, 4% noise was added and for $\alpha=1.77$, 5% noise was added. In order to illustrate the long tail, a relatively large system size of $N=25\,000$ was used for this part of the figure.

dynamics ($\varepsilon=0.14$). As clearly can be seen, the application of 10% noise yields almost the same results as applying no noise at all while a level of 5% noise strongly reduces the number of attractors for a fairly large interval of the nonlinearity. Indeed, from around $\alpha\approx1.63$ to around $\alpha\approx1.71$, the addition of 5% noise guides the system to the coherent attractor.

That this phenomenon is not restricted to some very specific values of the coupling strength ε can be seen in Fig. 5, where the average number of clusters versus ε is plotted for two values of the nonlinearity α. In Fig. 5(a), $\alpha=1.7$ was chosen; as for this value of the nonlinearity the difference between 5% and 10% is particularly big in Fig. 4, while in Fig. 5(b) $\alpha=1.85$ was chosen, since it is roughly the smallest value for the nonlinearity beyond $\alpha=1.6$ for which the noise levels make no difference in Fig. 4.

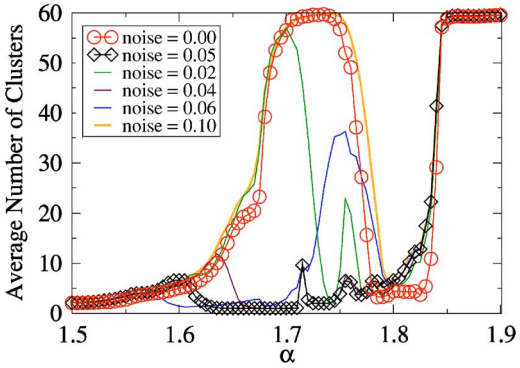

FIG. 4. (Color online). The average number of clusters versus the nonlinearity α for various noise levels applied in the same fashion as in Fig. 2(b). The noise level (5%) that yields the greatest overall reduction in the final number of clusters is marked by diamonds, while for comparison the case without added noise is marked with circles. The coupling strength was set to $\varepsilon=0.14$ and the average of 10^3 runs was taken for each data point.

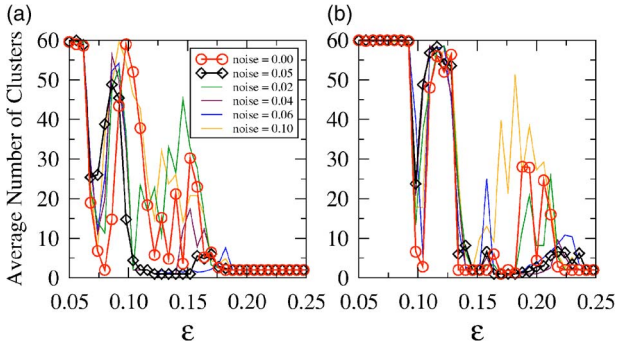

FIG. 5. (Color online). The average number of clusters versus the coupling strength ε for various noise levels applied in the same fashion as in Fig. 2(b). The noise level (5%) that yields the greatest overall reduction in the final number of clusters is marked by diamonds, while for comparison the case without added noise is marked with circles. The nonlinearity was set to $\alpha=1.7$ in (a) and $\alpha=1.85$ in (b) while the average of 10^3 runs was taken for each data point.

It can therefore be concluded that the drastic effect of temporarily adding noise displayed in Fig. 2(b) is not limited to a very specially tuned miniscule parameter region but occurs in a reasonably large region of parameter space.

IV. ATTRACTOR CONTROL

The results of the last section suggest that by adding suitable amounts of noise for some time, one can switch attractors such that the cluster number is eventually reduced one by one. Conversely, by adding a larger amount of noise, it is possible to desynchronize the elements and increase the cluster number. Thus controlled attractor selection is possible by just changing the noise strength and its duration.

To illustrate this, we have carried out the numerical experiment depicted in Fig. 6: After starting from random initial conditions and allowing for a transient of 10^5 time steps, a short "down-level" noise burst is applied for ten times ev-

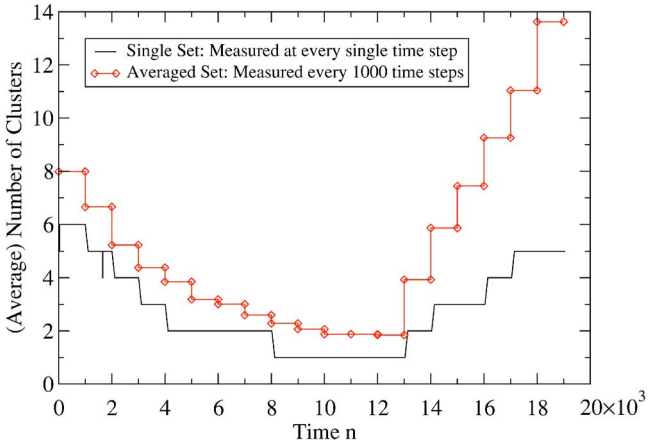

FIG. 6. (Color online). Noise-induced attractor switching for $\alpha=1.77$, $\varepsilon=0.14$, and $N=60$. The attractors are controlled by applying short noise bursts of 5% for reducing the cluster number and of 9% for increasing the cluster number.

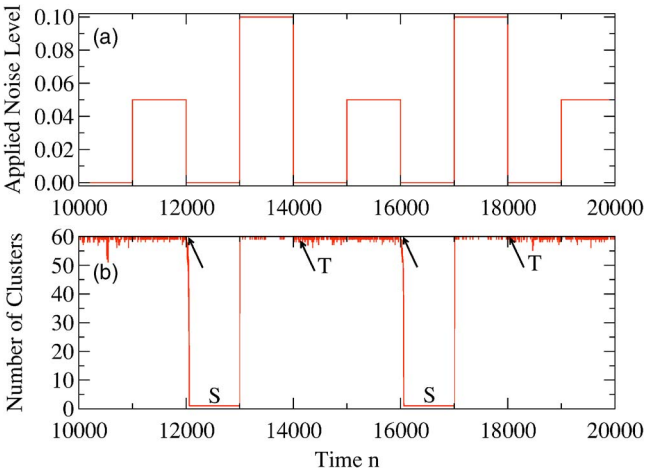

FIG. 7. (Color online). Deterministic binary switching of attractors. (a) depicts the level of applied noise while (b) graph shows the system's response. The arrows indicate the points where the attractor switches. The nonlinearity was set to $\alpha=1.85$, the coupling strength to $\varepsilon=0.15$, and the system size is $N=60$.

ery 10^3 time steps, and then from time 1.3×10^4 on, a short "up-level" noise burst is applied six times. The line marked with the circles represents the average number of clusters just before and just after applying the noise bursts over 10^3 runs. The "down level" for the noise is 5% and the "up level" is 9% while the "down-burst time" is 25 time steps and the "up-burst time" 5 steps. The solid black line shows a single run with the number of clusters determined at every time step. Again noise bursts are applied as for the averaged case, except that the "burst-up" time was five time steps and the "burst-down time" two time steps. An important point is that the noise is only required for the switching of the attractors and not for sustaining them once selected.

While individual runs in Fig. 6 may differ depending on the initial conditions, the binary switching depicted in Fig. 7 is completely independent of the state the system is in. That is, the switching is completely deterministic and hence could, in principle, be used for digital logic. This is achieved by applying the temporary noise long enough to assure that all the elements are either on the coherent attractor (5% noise) or mostly in the turbulent phase (10% noise). It should be noted that in this case too the noise is only necessary for the switch and not for the sustaining of a state.

As is known from the phase diagram Fig. 1 and can be seen from Figs. 4 and 5, the cluster number not only depends on the amount of noise, but also on the parameters. Consequently, instead of selecting an attractor by adding noise, one can also attempt to deterministically select attractors by changing (sweeping) parameter values. Indeed, Fig. 8 shows that this is possible and that the inverse of the sweeping speed corresponds to the noise duration time (i.e., a fast sweeping speed corresponds to a short noise burst). The dependence on the sweeping speed is relevant in applications since in experiments a change in an external condition requires some time before its effects are fully felt, and clearly systems in nature generally cannot jump from one parameter value to another. Furthermore, in this case, the attractor selection can be done without adding noise which may be es-

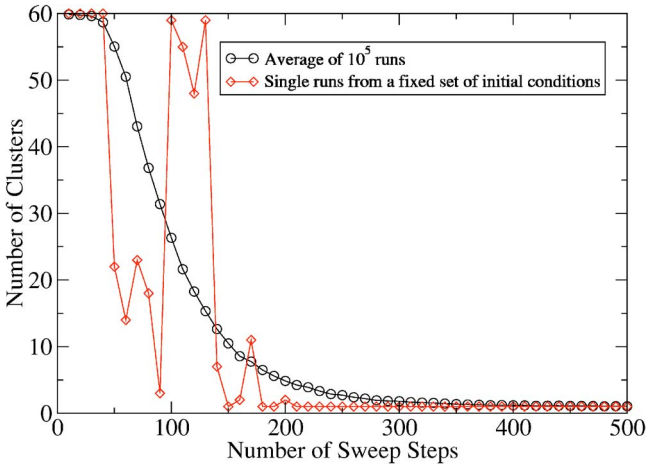

FIG. 8. (Color online). Effect of the ε sweep speed on the number of clusters in the model, Eq. (1). The x axis indicates the number of steps between $\varepsilon_{\text{start}}=0.05$ and $\varepsilon_{\text{end}}=0.14$. The nonlinearity is set to $\alpha=1.77$. At $\varepsilon_{\text{start}}$, a transient of 10^3 time steps was discarded. The average of 10^5 runs was taken for each data point indicated by a circle.

sential, as noise may not necessarily be available as a controlling factor.

V. MECHANISM

In a globally coupled system, the dynamic behavior of an attractor changes according to the clustering of its elements. Indeed, the change in the number of elements in a cluster is sometimes represented by a bifurcation diagram, as discussed in Ref. [9]. In that case, the stability *decreases* when the number of elements in the dominant cluster increases. However, in the model studied here, overall, the stability *increases* when the number of elements of in a synchronized cluster increases. This is illustrated in Fig. 9, where the split exponent, given by $\ln(1-\varepsilon)+1/T\Sigma_T f'(x_i)$ [9], is plotted versus the size of the largest cluster N_1. The increase in the size of N_1 is achieved in the same fashion as for Fig. 6 by applying a short noise burst every 1000 time steps. For the calculation of the split exponent, after every noise burst, a copy of

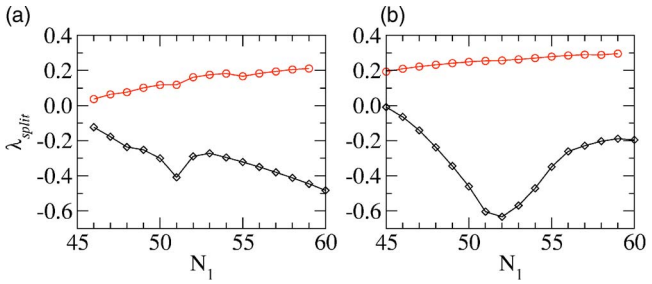

FIG. 9. (Color online). Split exponents versus the size of the largest cluster N_1. The lines with the diamonds indicate the split exponent of the elements belonging to N_1, while the lines with the circles give the average of the split exponents of the desynchronized elements. $N=60$. (a) $\alpha=1.67$, $\varepsilon=0.14$, noise=6%, burst time=20; (b) $\alpha=1.77$, $\varepsilon=0.14$, noise=5%, burst time=26.

the system state is made and, after identifying a synchronized or desynchronized element, evolved for 10^5 time steps only if N_1 is the only cluster while all the remaining elements are desynchronized. In case there is more than one cluster $N_j>1$, the copy is discarded and the split exponent not calculated. Overall data are collected from 10^5 runs. In Fig. 9(a), the increase in stability when $N_1\rightarrow N$ can clearly be seen, however in Fig. 9(b) (the same parameters as for Fig. 6), the stability appears to decrease. This is due to the fact that the periodicity of the band structure changes. In (a), from $N_1=46$ to $N_1=51$, the=periodicity is four; then at $N_1=52$ there is a transition to period two where the synchronized elements are somewhat more chaotic, and from $N_1=53$, the periodicity of the band structure is clearly two. In (b), on the other hand, the transition from the period-four to the period-two band structure is more extended, ranging from $N_1=52$ to $N_1=59$, and hence the final increase in stability is only found from $N_1=59$ to $N_1=60$. However, it can also clearly be seen that the split exponent of the desynchronized elements increases over the entire range depicted, indicating that these elements become more chaotic as the N_1 cluster becomes larger.

The increase in stability when N_1 approaches N can be understood by first considering the coherent map $x_{n+1}=(1-\varepsilon)f(x_n)+\varepsilon x_n$. It is easily shown that this map is in fact just a variable and parameter transform of the single logistic map such that

$$x_{n+1}=(1-\varepsilon)f(x_n)+\varepsilon x_n, \tag{2}$$

$$\Leftrightarrow x'_{n+1}=1.0-\alpha' x'^2_n,$$

$$x'=kx+d,$$

$$d=\frac{-2\varepsilon}{4\alpha(1-\varepsilon)^2-(2-\varepsilon)\varepsilon},$$

$$k=\frac{4\alpha(1-\varepsilon)}{4\alpha(1-\varepsilon)^2-(2-\varepsilon)\varepsilon},$$

$$\alpha'=\alpha(1-\varepsilon)^2-\frac{1}{4}(2-\varepsilon)\varepsilon. \tag{3}$$

Hence, in the completely synchronized case, the coupling reduces the effective nonlinearity α'. When the system is not completely synchronized, Eq. (2) for the synchronized elements and its corresponding effective nonlinearity can be expressed as

$$x_{n+1}^{Sync}=(1-\varepsilon)f(x_n^{Sync})+\frac{N_1}{N}\varepsilon x_n^{Sync}+\kappa, \tag{4}$$

$$\alpha'=\alpha(\kappa+(1-\varepsilon)^2-\kappa\varepsilon)-\frac{1}{4}\left(2-\frac{N_1}{N}\varepsilon\right)\frac{N_1}{N}\varepsilon, \tag{5}$$

where κ is the contribution of the remaining (desynchronized) terms. Hence, the closer N_1 gets to N, the smaller the effective nonlinearity.

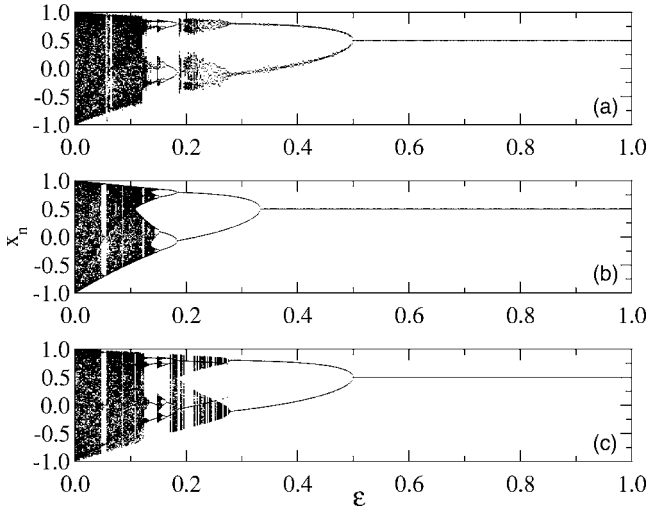

FIG. 10. Bifurcation diagrams of Eq. (1), its coherent version, and Eq. (6), where the local map is the logistic map $f(x_n)=1-2.0x_n^2$. (a) depicts the linearly coupled logistic lattice Eq. (1); (b) depicts the coherent version of Eq. (1); and (c) depicts the two-band map, Eq. (6).

Summing up, as N_1 increases, the effective nonlinearity of the synchronized state decreases and the instability of the desynchronized elements increases. This provides one part of the explanation as to why the system can step through successive attractors when increasing N_1.

In order to further investigate the mechanism underlying the reported behavior, bifurcation diagrams for Eqs. (1) and its coherent version are plotted in Figs. 10(a) and 10(b).

In this context, it should be emphasized that in the parameter region we have studied for attractor selection, given the present type of coupling, the synchronized state is nonchaotic (i.e., it is of period 2, 4,…), and that chaos appears only in many-cluster states. Indeed, this can be seen clearly in Fig. 10, where the globally coupled map, Fig. 10(a), bifurcates well before the synchronized map, Fig. 10(b).

The simplest nonuniform states are obtained when elements are attracted to different temporal phases of the uniform period-two state. When starting from random initial conditions, one would expect roughly half the elements to be attracted to each of the two temporal phases. This allows us to construct the two-band map defined as

$$x_{n+1} = (1-\varepsilon)f(x_n) + \frac{\varepsilon}{2}(x_n + y_n),$$

$$y_{n+1} = (1-\varepsilon)f(y_n) + \frac{\varepsilon}{2}(x_n + y_n), \tag{6}$$

whose bifurcation diagram is given in Fig. 10(c).

The bifurcation diagram of the two-band map is found to qualitatively overlap well with the bifurcation diagram of model Eq. (1) and thus leads to the following explanation of the observed phenomena.

The unequal maps applied to the local and coupled terms lead to a relative shift between the bifurcation cascades of the synchronized and nonsynchronized systems such that the synchronized system still has periodic attractors when the nonsynchronized system falls into a multiband chaotic regime. As the chaotic bands are separated by a repellor, a multiband attractor cannot move toward the more stable synchronized attractor. With the addition of a sufficient amount of noise, however, sites can occasionally cross the repeller and the number of sites in the same band increases (these crossings can, of course, be both ways, however, as the distances between the attracting and repelling orbits are unequal, there will be a bias). Once the sites are in the same band and the noise is switched off, they will rapidly synchronize. Since an orbit has to cross the repeller for the switching, the noise magnitude needs to exceed the distance between an orbit of an element and the repeller. On the other hand, if the noise is too large, the asymmetry mentioned above is rendered irrelevant. Hence, in order to obtain a switch to a state with more synchronized elements the noise needs to be larger than the distance between the repeller and one of the bands while smaller than the distance between the repeller and the other band. The 5% noise discussed in Sec. III is such an optimal noise strength. When switching to a more desynchronized state, the noise needs to exceed the distances between the repellor and both bands. For this a good value is 10% noise, but of course this value can be made larger.

Above we found that when, for a given set of parameters, a stable synchronized state exists, an attractor consisting of synchronized elements and desynchronized chaotic elements will show a decrease in orbital instability as the number of elements in the synchronized cluster increases (given that the periodicity of the band structure is equal). In the globally coupled map, Eq. (1), these features are expected to hold when $(1-\epsilon)f(x)+\epsilon g(x)$ has a stable fixed point or is periodic and $(1-\epsilon)f(x)$ is chaotic. This was verified by investigating some variations of the maps employed thus far.

First, the logistic map was replaced by a sine map of the form

$$x_{n+1} = f(x_n) = \sin(2\pi x_n) \tag{7}$$

which, as opposed to the logistic map's single local maximum, has two local maxima and two local minima for $x_n \in [-1,1]$. The relevant bifurcation diagrams are shown in Fig. 11, and indeed noise-induced synchronization can again be found (e.g., for $\varepsilon=0.15$) for parameters where the composed map has chaotic multiband attractors and the coherent map temporally periodic attractors.

Second, the linear coupling was replaced such that a different map is applied to the coupled terms than to the local term. In other words, the model was modified to become

$$x_{n+1}^i = (1-\varepsilon)f(x_n^i) + \frac{\varepsilon}{N}\sum_{j=1}^{N} \sin\left(\frac{2\pi}{3}x_n^j\right), \tag{8}$$

where $\sin[(2\pi/3)x_n]$ is a sine-type map that is nearly linear around $x_n=0$ and has a small local minimum and maximum at $x_n=-2/3$ and $x_n=2/3$, respectively. Again, noise can be used to switch a chaotic multiband attractor to the synchronized nonchaotic attractor (e.g., for $\alpha=1.8$, $\varepsilon=0.18$, and a noise level of 3%).

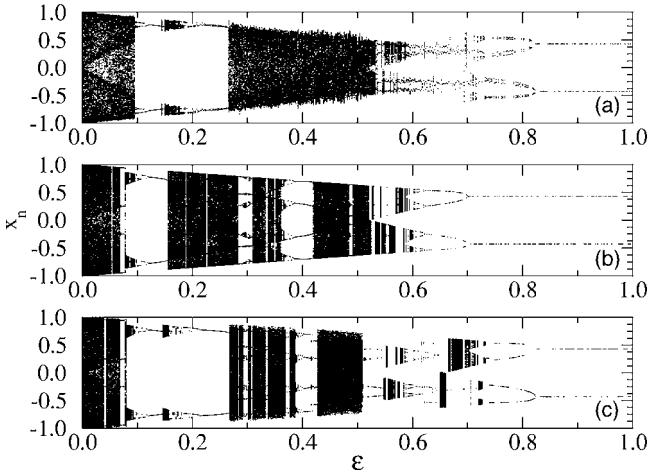

FIG. 11. Bifurcation diagrams of Eqs. (1), (2), and (6), where the local map is the sine map $f(x_n)=\sin(2\pi x_n)$. Panel (a) depicts the linearly coupled sine map lattice, Eq. (1); (b) the coherent map, Eq. (2); and (c) the two-band map, Eq. (6).

Therefore, it is conjectured that the observed behavior is rather general for systems where the dynamics of the single element $f(x_n^i)$ is chaotic and the coupling leads to desynchronization with chaos. Indeed, one could expect that it may also be common in systems of globally coupled ODEs, or in experiments. For example, the experiment of globally coupled chaotic chemical oscillators by Hudson *et al.* [21] might be modified in such a way that noise-induced coherent synchronization of potentially chaotic elements can occur.

VI. CONCLUSION

As discussed in the Introduction, the selection of specific attractors in multiattractor systems by inputs is important in biological problems like neural networks, cell states given by gene networks, and so forth. The attractor selection presented here is simply achieved by the strength and duration time of noise, or by the speed of sweeping parameters. No tuning mechanism is required. Considering the generality of the mechanism, it will be interesting to see possible applications of the mechanism to biological problems, as well as applications to information processing.

To conclude, while in the earlier studies of GCM chaotic instability is strong when elements are synchronized, here the scenario is reversed as the synchronized dynamics is nonchaotic and chaotic instability is introduced through the coupling term. A striking consequence of this setup is that attractors can effectively be controlled by external inputs. The underlying mechanisms are found to be quite generic and the introduced model can therefore serve as a simple prototype for controlled attractor switching in high-dimensional systems.

Indeed, we surmise that in general the following circumstances should be sufficient in order for a globally coupled system to display the dynamics described in this paper: the coexistence of a stable nonchaotic synchronized state with a chaotic desynchronized state such that the global coupling term enhances the orbital instability.

ACKNOWLEDGMENTS

This work is partially supported by a Grant-in-Aid for Scientific Research (11CE2006) from the Ministry of Education, Science, and Culture of Japan. Furthermore, FHW is especially grateful for support by the Hitachi Scholarship Foundation. We would also like to thank K. Yanagida for his collaboration during the early stages of this work.

[1] H. Gutfreund and G. Toulouse, in *Biology and Computation: A Physicist's Choice* (World Scientific, Singapore, 1994).
[2] S. Kauffman, *The Origin of Order* (Oxford University Press, Oxford, 1993).
[3] K. Kaneko and T. Yomo, J. Theor. Biol. **199**, 243 (1999).
[4] J. N. Onuchic, P. G. Wolynes, Z. Lutheyschulten, and N. D. Socci, Proc. Natl. Acad. Sci. U.S.A. **92**, 3626 (1995).
[5] S. Kauffman, J. Theor. Biol. **22**, 437 (1969).
[6] K. Kaneko, in *Theory and Applications of CA*, edited by S. Wolfram (World Scientific, Singapore, 1986), pp. 367–399.
[7] F. H. Willeboordse and K. Kaneko, Phys. Rev. Lett. **73**, 533 (1994).
[8] S. Ishihara and K. Kaneko, J. Phys. Soc. Jpn. **71**, 2357 (2002).
[9] K. Kaneko, Physica D **41**, 137 (1990).
[10] K. Kaneko, J. Phys. A **24**, 2107 (1991).
[11] A. Crisanti, M. Falcioni, and A. Vulpiani, Phys. Rev. Lett. **76**, 612 (1996).
[12] O. Popovych, A. Pikovsky, and Y. Maistrenko, Physica D **168**, 106 (2002).
[13] S. Manruiba and A. Mikhailov, Europhys. Lett. **53**, 451 (2001).
[14] M. Mezard, G. Parisi, and M. Virasoro, *Spin Glass Theory and Beyond* (World Scientific, Singapore, 1987).
[15] K. Kaneko and I. Tsuda, *Complex Systems: Chaos and Beyond—A Constructive Approach with Applications in Life Sciences* (Springer-Verlag, Berlin, 2003); "Focus issue on chaotic itinerancy," Chaos **13**, 926 (2003).
[16] K. Kaneko, Phys. Rev. Lett. **78**, 2736 (1997).
[17] E. Mosekilde, Y. Maistrenko, and D. Postnov, *CHAOTIC SYNCHRONIZATION: Applications to Living Systems* (World Scientific, Singapore, 2002).
[18] K. Kaneko, Physica D **124**, 322 (1998).
[19] S. Kraut, U. Feudel, and C. Grebogi, Phys. Rev. E **59**, 5253 (1999).
[20] S. Sinha, Phys. Rev. E **66**, 016209 (2002).
[21] I. Z. Kiss, Y. Zhai, and J. L. Hudson, Phys. Rev. Lett. **88**, 238301 (2002).